

# Time Dependence of Bed Particle Layer Formation in Fluidized Quartz Bed Combustion of Wood-Derived Fuels

Hanbing He,<sup>\*,†</sup> Dan Boström,<sup>‡</sup> and Marcus Öhman<sup>†</sup>

<sup>†</sup>Energy Engineering, Division of Energy Science, Luleå University of Technology, SE-971 87 Luleå, Sweden

<sup>‡</sup>Energy Technology and Thermal Process Chemistry, Umeå University, SE-901 87 Umeå, Sweden

**ABSTRACT:** Formation of sticky layers on bed particles has been considered as a prerequisite for bed agglomeration in fluidized bed combustion of wood-derived fuels. The present investigation was undertaken to determine the quartz bed particle layer formation process in fluidized bed combustion of wood-derived fuels. Bed material samples from three different appliances, bench-scale bubbling fluidized bed, full-scale bubbling fluidized bed, and full-scale circulating fluidized bed, at different sampling times from startup with a fresh bed were collected. Scanning electron microscopy/energy-dispersive spectroscopy (SEM/EDS) and X-ray diffraction (XRD) were used to explore layer morphology and chemical composition and to gain information on crystalline phases of the layers and coatings. Significant differences in layer morphology and composition were found for quartz bed particles with different ages. For bed samples with operational duration of less than 1 day, only one thin Ca-, Si-, O-, and K-rich homogeneous quartz bed particle layer that has a relatively high K/Ca molar ratio was found. For quartz bed particles with an age from around 1 day to 2 weeks, an outer more particle-rich coating layer was also found. During the initial days of this period, the layer growth rate was high but decreased over time, and decreasing K/Ca and increasing Ca/Si molar ratios in the inner bed particle layer were observed. For bed particles with age between 2 and 3 weeks, a much lower layer growth rate was observed. At the same time, the Ca/Si molar ratio reached high values and the K concentration remained on a very low level. In addition to these layer formation processes mentioned, also an inner–inner/crack layer was also formed in the circulating fluidized bed quartz bed particles simultaneously with the inner bed particle layer.

## 1. INTRODUCTION

Biomass fuels, provided for potentially renewable and CO<sub>2</sub>-neutral energy sources, have been used widely during recent decades. Fluidized bed combustion (FBC) is considered as one of the most suitable technologies for heat and power production, because of high fuel flexibility, low process temperature, and emission control. However, bed agglomeration could be one potential operational problem, which may lead to a non-scheduled shutdown of the combustion plant in severe cases with significant economic losses. Although frequent bed change is a potential measure for reducing the bed agglomeration risk for some fuels, it definitely brings about additional cost and is not economically sustainable on a long-term basis. In general, any predictive methodologies for assessing the agglomeration tendency are important for operated reactors.

To understand agglomeration phenomena in the FBC, extensive bed particle layer analysis was performed on quartz particles.<sup>1–6</sup> Most FBC processes are run with natural sand mainly consisting of quartz.<sup>7,8</sup> The bed agglomeration mechanisms during FBC of biomass fuels in a quartz bed were summarized by Brus et al.,<sup>9,10</sup> De Geyter et al.,<sup>11</sup> and Grimm et al.,<sup>2</sup> who concluded that the agglomeration proceeds with an initial bed particle layer formation, followed by subsequent viscous flow sintering and agglomeration for fuels rich in Ca and K, i.e., wood-derived fuels, or direct adhesion of bed particles by partly molten ash-derived silicates or phosphates for fuels rich in Si and/or P, e.g., straws and agricultural residues. Coating/layer-induced bed agglomeration has been suggested to be the main route for agglomeration in

combustion of woody biomass fuels. Multiple layers with different properties and compositions have often been found around bed particles during combustion of biomass.<sup>9,12–14</sup> It appears that the inner layer compositions depend upon the composition of both the bed and the fuel, whereas the outer layers are more related to the fuel ash compositions.<sup>7,9,11,14,15</sup>

The formation of sticky layers on bed particles has been thought to be the prerequisite for agglomeration in combustion of woody fuels. The ash compounds formed during the fuel conversion can be attached to the bed material by a combination of deposition of small ash particles on the bed particle surface, condensation, and chemical reaction of gaseous alkali metal species.<sup>13,16</sup> Nuutilainen et al.<sup>14</sup> indicated that the coating layers containing potassium or sodium may be adhesive and cause the formation of agglomerates. Zevenhoven-Onderwater et al.<sup>17</sup> suggested that the interaction of potassium containing easily soluble (reactive) components in the fuel with the silica-rich bed was the first and critical step in the buildup of a layer on the bed material, which captured other small ash particles, forming a sticky layer. Thy et al.<sup>18</sup> also concluded that the initial interaction between bed particles and potassium compounds likely carried by the flue gas or aerosols results in a continuous surface reaction zone around bed particles without enlargement of the particles.

During recent decades, most research on FBC regarding bed agglomeration has been focused on bed particle layer

Received: February 12, 2014

Revised: May 8, 2014

Published: May 8, 2014

**Table 1.** Summary of the Bed Material and Operational Data for the Sampling Campaign

plant	abbreviation	bed mass (ton)	bed consumption (wt % of bed/day)	average bed particle size ( $\mu\text{m}$ )	bed temperature (°C)	fuel	campaign duration (days)
bench-scale BFB at 5 kW	BFB5	0.0005	0	106–125	800	bark	1.7
full-scale BFB at 30 MW <sub>th</sub>	BFB30	20	<3	700	800–880	10% bark, 30% logging residues, and 40% wood chips	23
full-scale CFB at 122 MW <sub>th</sub>	CFB122	20–25	50	280	840–880	40% bark and 60% sawdust + logging residues	6

characteristics of relatively mature bed particles. However, only limited studies are found on bed particle layer buildup and composition as a function of time, starting from fresh bed material. Brus et al.<sup>19</sup> reported that the initial growth rate for the bed particle coating was a few micrometers per day but decreased in time. In addition, the critical thickness was reached within a few days and determined to be relatively thin (<10  $\mu\text{m}$ ). Visser et al.<sup>20</sup> studied the chemical characteristics and morphologies of bed particles collected after different operational times during lab-scale fluidized bed wood combustion and concluded that the coating thickness increased over time and with increasing ash content of the fuel. The objective of the work was to determine the coating/layer formation processes on quartz bed material during FBC of typical wood-derived fuels (in this work, represented by fuel mixtures of soft wood bark, different assortments of stem wood, and logging residues from soft wood). The bed samples were collected at different times from startup with a fresh bed during both laboratory experiments and full-scale boiler experiments. The morphologies and elemental composition of the bed particle layers and coatings were examined by scanning electron microscopy/energy-dispersive spectroscopy (SEM/EDS). Semi-quantitative information on the crystalline phases in bed particle layers was obtained with X-ray diffraction (XRD).

## 2. MATERIALS AND METHODS

The methodologies used in the present study included the following: (1) bed material sampling at different times during controlled bench-scale FBC tests of bark, (2) bed material sampling at different times from full bed change during full-scale combustion tests of wood-based fuel mixtures, and (3) SEM/EDS and XRD analyses of collected bed material samples, to determine the growth and change of composition of the coatings/layers as a function of time.

**2.1. Bed Material Sampling with a Bench-Scale Bubbling Fluidized Bed (BFB) at 5 kW.** Controlled FBC tests, described in detail elsewhere,<sup>21</sup> were performed with bark as fuel, using quartz sand (>98% quartz) with a size fraction of 106–125  $\mu\text{m}$ . These relatively small bed particle sizes were chosen to facilitate the determination of the coating/attack layer thickness of the bed particles. The primary airflow was set to 80 NL/min and kept constant during the experiments. The fluidization velocity was kept 10 times higher than the minimum fluidization velocity, corresponding to ~1 m/s. The reactor was heated by external wall heating elements and preheated primary air. During heating of the reactor, the bed material was introduced gradually and fluidized all of the time. The pelletized fuel was introduced into the reactor after reaching the desirable bed temperature. A total of 540 g of bed material was used. A bed temperature of 800 °C and excess oxygen concentration of 6% in the flue gases were maintained throughout the experiment. Bed material samples were collected after different lengths of time from startup (4, 8, 16, 24, 32, and 40 h).

**2.2. Bed Material Sampling with a Full-Scale BFB at 30 MW<sub>th</sub>.** Bed material samples were collected from a 30 MW<sub>th</sub> BFB (Ahlström). The fuel consisted of a typical wood-based mixture, with an ash composition relatively similar to the bark fuel used in the

bench-scale experiments. Sand material (>80% quartz) with an average particle size of 700  $\mu\text{m}$  was used as bed material. Bed material samples (about 1 kg) were collected under normal operation conditions after 1, 3, 5, 13, and 23 days from completed bed change at startup. The bed material was exchanged at the same rate as that during normal operation (see Table 1 for further details).

**2.3. Bed Material Sampling with a Full-Scale Circulating Fluidized Bed (CFB) at 122 MW<sub>th</sub>.** Bed material samples (about 1 kg) were also collected from a 122 MW<sub>th</sub> CFB (Foster Wheeler), after different operation times (3, 4, and 6 days) from completed bed change at startup. Sand material (>80% quartz) with an average particle size of 280  $\mu\text{m}$  was used as the bed material. Wood-based fuel mixtures, with an ash composition relatively similar to the bark fuel used in the bench-scale experiments, were used. The bed material was changed to the same extent as that during normal operation (see Table 1 for further details).

The same type of fuel was used for the entire sampling campaign in each full-scale plant, and the operating conditions were kept as normal and constant as possible. This was verified by logged operation data as well as semi-continuously determined fuel ash and moisture data. The fuel characteristics for all used fuels are shown in Table 2.

**Table 2.** Fuel Characteristics of the Main Ash-Forming Elements and Ash Content

	BFB5	BFB30	CFB122
ash content (wt % dry substance)	3.0	1.8 ± 0.51	3.1 ± 0.47
ash-forming elements (wt % dry substance)			
Si	0.21	0.12	0.20
Al	0.036	0.019	0.041
Ca	0.83	0.44	0.76
Fe	<0.082	0.12	0.033
K	0.19	0.11	0.18
Mg	0.065	0.040	0.062
Na	<0.036	0.010	0.016
P	0.037	0.027	0.042
S	0.030	0.023	0.033
Cl	<0.010	<0.010	0.010

**2.4. SEM/EDS and XRD Analyses of Bed Material.** Bed samples from full-scale experiments were sieved gently, and bed particles from BFB at 30 MW<sub>th</sub> and CFB at 122 MW<sub>th</sub> with the size of 500–850 and 200–355  $\mu\text{m}$  were collected, respectively. Bed samples from bench-scale experiments were not sieved because of the uniform bed material used. The collected bed particles were mounted in epoxy resin, and then the blocks of epoxy resin were polished to obtain cross-sections of the bed material grains. The bed particles were thereafter analyzed with SEM/EDS. To minimize the effects of non-central cross-sections and the varying “particle age” because of the continuous bed change in the full-scale plants, only the largest bed particle cross-sections with the thickest layers were analyzed.

More than 10 typical quartz particles were analyzed for each sample, and four spots evenly distributed over the periphery of the bed particle were chosen for estimation of layer thickness. Where bed particle layers were found, inner layers and outer coating layers were analyzed separately. Inner layers and outer coating layers were discerned visually on the SEM image of the cross-sections, and spots for elemental

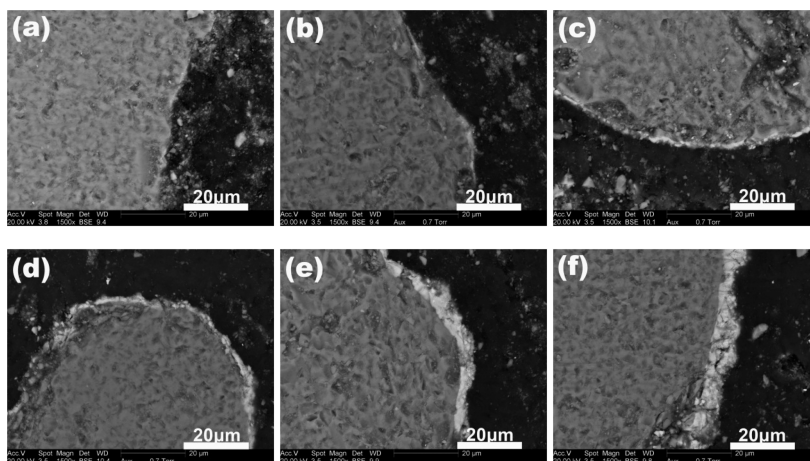


**Figure 1.** SEM images of typical cross-sections of bed particle layers found in bed samples taken from BFB at 5 kW versus operation times of (a) 4 h, (b) 8 h, (c) 16 h, (d) 24 h, (e) 32 h, and (f) 40 h from completed bed change at startup.

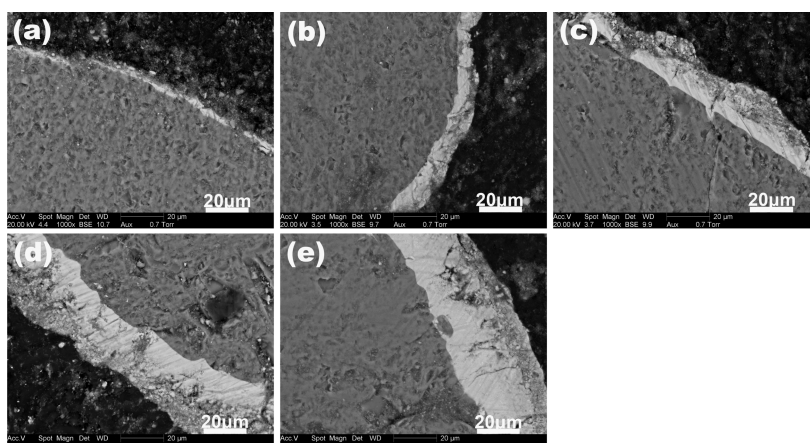


**Figure 2.** SEM images of typical cross-sections of bed particle layers found in bed samples taken from BFB at 30 MW<sub>th</sub> versus operation times of (a) 1 day, (b) 3 days, (c) 5 days, (d) 13 days, and (e) 23 days from completed bed change at startup.

analysis were chosen in the middle of each layer. To determine elemental composition of the formed bed particle layers, 2–3 EDS spot analyses evenly distributed for each quartz particle layer were chosen. Where the layers were thin, the influence of the bed material on the analysis results cannot be totally excluded because of the limited spatial resolution for quantification with SEM/EDS (a few micrometers).

The bed particles collected from bed materials sampled after 3, 5, 13, and 23 days from full-scale BFB at 30 MW<sub>th</sub> and 6 days from CFB at 122 MW<sub>th</sub> were analyzed without grinding by XRD with a D8 Advance (Bruker AXS, Karlsruhe, Germany). Cu K $\alpha$  radiation with a nickel filter and a Vantec-1 detector were used. The samples were measured by continuous scan mode between 10° and 70° in 20°. Diffrac<sup>plus</sup> EVA<sup>22</sup> with the PDF-2 database<sup>23</sup> was used to make initial qualitative identifications. Further analysis was performed in Diffrac<sup>plus</sup> TOPAS<sup>24</sup> using Rietveld refinement techniques with reference data from Inorganic Crystal Structure Database (ICSD)<sup>25</sup> to make a semi-quantitative analysis of the crystalline matter in these samples. The penetration depth of the X-ray can be determined using the known absorption coefficient and mass density of the material.<sup>26</sup> The penetration depth of X-ray in Si and Ca is 61 and 43 μm, respectively. From XRD and EDS results of the layers, it is reasonable to assume that the mass composition is 60% Ca and 40% Si without considering other elements. On the basis of that, the penetration depth of the X-ray calculated is 77 μm.

### 3. RESULTS

**3.1. Bed Particle Layer Morphology.** Typical illustrations of cross-sections of the bed particle layers from different bed samples collected from bench-scale experiments are shown in Figure 1. From the backscattered electron images in panels a–f of Figure 1, a layer can be distinguished around the bed particles as a lighter periphery surrounding the darker bed particles. In bench-scale samples (less than 40 h), only one bed particle layer was found. Only limited parts of the bed particle surfaces are covered by lighter material for the samples taken after 4 and 8 h (panels a and b of Figure 1).

For samples taken from BFB at 30 MW<sub>th</sub>, with different sampling times from 1 day to 23 days, all bed particles were found to be surrounded by layers (Figure 2). Only one layer around the bed particles was observed for samples with an age of 1 day (Figure 2a). For bed particles with ages of 3, 5, 13, and 23 days, on the other hand, the accumulated material surrounding the bed particles was found to consist of an inner layer and an outer coating layer (panels b–e of Figure 2). The inner layers are more homogeneous, whereas the outer layers are more heterogeneous and particle-rich, in agreement with previous results from the full-scale combustion of woody biomass.<sup>9</sup> It is clear that the total layer thickness increases with increasing bed particle age.

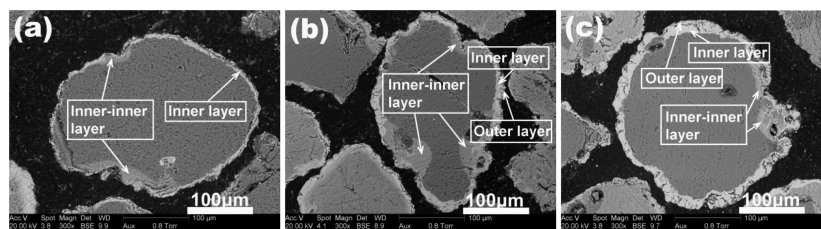


**Figure 3.** SEM images of typical cross-sections of bed particles found in bed samples taken from CFB at 122 MW<sub>th</sub> versus operation times of (a) 3 days, (b) 4 days, and (c) 6 days from completed bed change at startup.

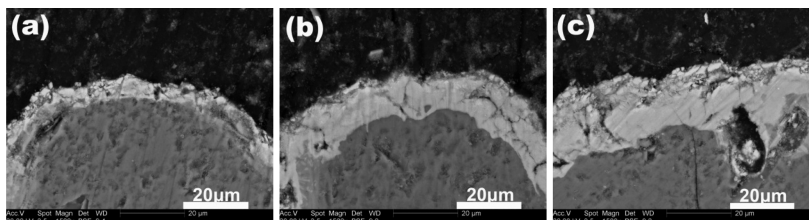


**Figure 4.** SEM images of typical cross-sections of bed particle inner and outer layers found in bed samples taken from CFB at 122 MW<sub>th</sub> versus operation times of (a) 3 days, (b) 4 days, and (c) 6 days from completed bed change at startup.

Typical illustrations of cross-sections of the bed particle surfaces from different bed samples taken from CFB at 122 MW<sub>th</sub> are shown in Figure 3. In addition to the inner layer and outer coating layer (lighter), a gray layer was also observed between the bed particle surface (darker) and the inner layer (panels a–c of Figure 3). This gray layer was defined here as an inner–inner layer and can usually be found in the vicinity of relatively thin inner layers or cracks rather than around the whole bed particle surface. The outer layer is less obvious in the bed samples taken after 3 days of operation (Figure 4a). For bed particles with ages of 4 and 6 days, the outer coating layer can be found but their thickness is much thinner compared to the inner as well as inner–inner layers (panels b and c of Figure 4).

**3.2. Bed Particle Layer Composition.** To quantify the elemental composition of the different layers/coatings, a large number of EDS spot analyses were performed on each bed particle. Each bar represents the average composition of more than 20 spot analyses taken from different bed particle layers.

The element Si was excluded from the analyses shown in panels a and b of Figure 5, i.e., for samples taken from BFB at 5 kW to avoid possible influence from other parts than the thin layer because of limited spatial resolution. Besides, to avoid possible effects of fine K-rich particles mainly presented as KCl attached to the bed particle surface, the results of elemental analyses for samples after 4 and 8 h were classified according to the Cl content (Figure 5a). The results with Cl molar contents less than 1% were used as layer compositions. The results in Figure 5 show that the layers on the quartz bed particle mainly consist of Ca (except O and Si). Relatively high K and low Ca contents can be found for samples taken after 4 and 8 h compared to samples collected after a longer time from startup. It seems that the layer composition is similar for samples taken after 16, 24, 32, and 40 h (Figure 5b).

For samples from BFB at 30 MW<sub>th</sub>, the results in Figure 6 show that the inner layers on the quartz bed particles mainly consist of Ca and Si (except O), while the outer coating layers are dominated by Ca, Si, and Mg (except O) and seem to resemble the fuel ash composition more. The Ca content in the inner layers increased over time, but nevertheless, no major difference in the elemental composition for the outer layers

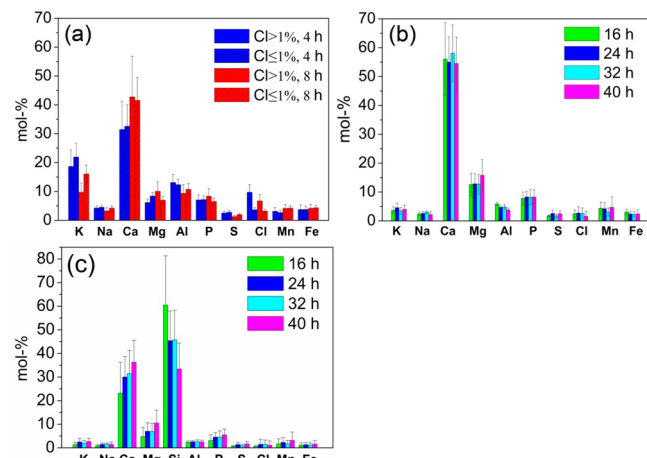


**Figure 5.** Average element composition with standard deviations on a C-, O-, and Si-free basis of the layers formed around quartz bed particles in BFB at 5 kW versus times at (a) 4 and 8 h and (b) 16, 24, 32, and 40 h and average element composition on a C- and O-free basis at (c) 16, 24, 32, and 40 h.

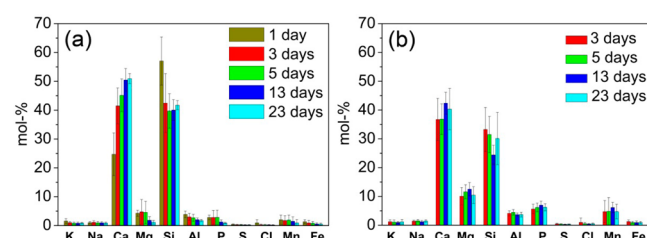


**Figure 6.** Average element composition with standard deviations on a C- and O-free basis of the (a) inner layer and (b) outer layer formed around quartz bed particles in BFB at 30 MW<sub>th</sub> at different times.

could be distinguished between samples taken after different lengths of the experiment (Figure 6b).

The elemental compositions of the inner–inner and inner layers for samples taken from CFB at 122 MW<sub>th</sub> are shown in Figure 7. The results show that the inner–inner layers are dominated by Si, K, and Ca (except O). The K and Ca contents

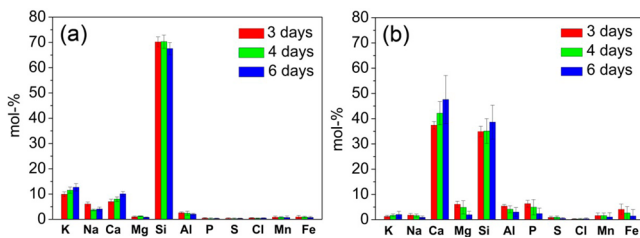


**Figure 7.** Average element composition on a C- and O-free basis and standard deviation of the (a) inner-inner layer and (b) inner layer formed around quartz bed particles in CFB at 122 MW<sub>th</sub> at different times.

of inner-inner layers increased over time, while the Si content remained almost constant (Figure 7a). The inner layers mainly consist of Ca and Si (except O). The concentration of the other elements than Ca, Si, and K in inner layers decreased over time.

The K/Ca molar ratio of the inner layers for BFB at 5 kW, BFB at 30 MW<sub>th</sub>, and CFB at 122 MW<sub>th</sub> samples at different sampling times is illustrated in Figure 8. For samples collected

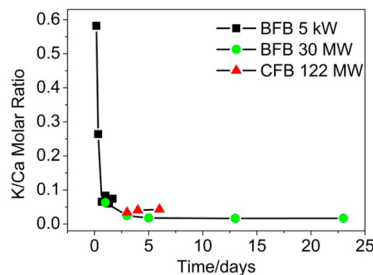


**Figure 8.** K/Ca molar ratio of the inner layers for BFB at 5 kW samples, BFB at 30 MW<sub>th</sub> samples, and CFB at 122 MW<sub>th</sub> samples as a function of the bed particle age.

after 4 and 8 h from bench-scale experiments, the K/Ca molar ratio is quite high but significantly reduced to a lower and similar level for samples collected after 16, 24, 32, and 40 h of operational time. For BFB30 samples, the K/Ca molar ratio decreased with increasing time until the 5 day samples, and after that, it remained close to constant over time. It should be noticed that BFB5 and BFB30 samples with similar sampling times, around 1 day, have similar K/Ca molar ratios. This ratio for samples from CFB122 is slightly higher compared to BFB30 samples collected after a similar time.

The collected bed samples taken after 3, 5, 13, and 23 days from BFB30 and 6 days from CFB122 were further analyzed with XRD to identify crystalline phases (Table 3). A number of phases were observed: oxides, calcite, anhydrite, apatite, and Ca manganate, probably reflecting the content of the outermost layer, leucite and Ca and Ca-Mg silicates probably reflecting the composition of the inner layer, and quartz and feldspars reflecting the original bed particles.

**3.3. Bed Particle Layer Thickness.** A large number of measurements were conducted on each bed sample to determine the average layer thickness. Figure 9a displays the layer thickness measured for bed particles from BFB experiments of different ages. The layer thickness of bed particles with ages of 4 and 8 h was not measured because of discontinuous and too thin bed particle surface layers. The layer thickness increased from 1 to 5 µm between 16 and 40 h from startup, giving a layer growth rate of 4 µm per day during this period. As illustrated in Figure 9b, the measured average total

**Table 3.** Crystalline Phases in Weight Percentage Identified with XRD for BFB30 with Sampling Time of 3, 5, 13, and 23 Days and CFB122 Samples with Sampling Time of 6 Days, Respectively

phases	BFB 30 3 days	BFB 30 5 days	BFB 30 13 days	BFB 30 23 days	CFB 122 6 days
CaSO <sub>4</sub>					2
CaCO <sub>3</sub>				3	3
CaO			1	2	
MgO	2	3	6	7	4
Ca <sub>5</sub> (PO <sub>4</sub> ) <sub>3</sub> (OH)	3	4	10	14	1
CaMnO <sub>3</sub>	2	1	2	11	
SiO <sub>2</sub>	40	48	25	25	35
NaAlSi <sub>3</sub> O <sub>8</sub>	8	5	3	2	8
KAlSi <sub>3</sub> O <sub>8</sub>	15	8	9	2	8
KAlSi <sub>2</sub> O <sub>6</sub>	2	4	3	2	11
CaSiO <sub>3</sub>	5	3	3	3	10
Ca <sub>3</sub> Mg(SiO <sub>4</sub> ) <sub>2</sub>	3	6	10	11	3
Ca <sub>2</sub> MgSi <sub>2</sub> O <sub>7</sub>				1	4
Ca <sub>2</sub> SiO <sub>4</sub> ( $\beta$ )	6	7	12	14	6
Ca <sub>2</sub> SiO <sub>4</sub> ( $\alpha$ )	6	4	9	3	3
Ca <sub>3</sub> SiO <sub>5</sub>	7	7	3	6	5

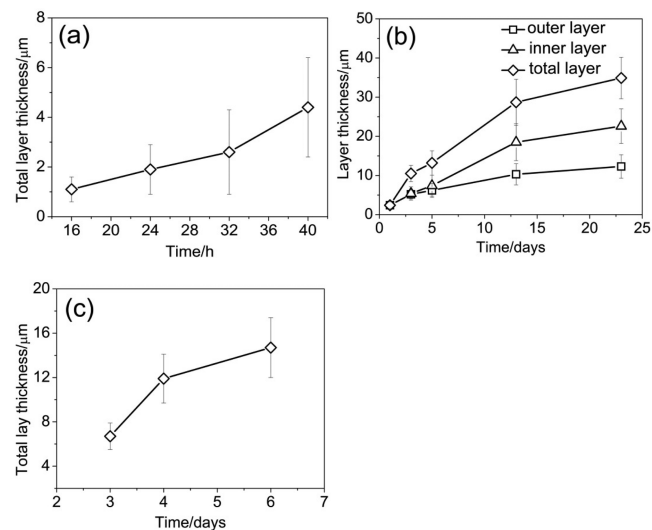


**Figure 9.** Average values of the measured layer thickness as a function of time of bed sampling for the (a) BFB at 5 kW samples, (b) BFB at 30 MW<sub>th</sub> samples, and (c) CFB at 122 MW<sub>th</sub> samples (excluding inner-inner layer thickness).

layer thickness is 2, 11, 13, 29, and 35 µm for samples from BFB30 after 1, 3, 5, 13, and 23 days, respectively. It is clear that the initial layer growth rate is relatively high, with a few micrometers per day, but decreasing over time to an accumulated total thickness of about 35 µm after 23 days. Figure 9c shows the measured average total layer thickness as a function of time for the bed sampling for CFB at 122 MW<sub>th</sub> bed samples (excluding inner-inner layer thickness). The layer thickness, excluding inner-inner layer thickness, was 5 µm after 3 days and increased to 13 µm after 6 days.

#### 4. DISCUSSION

The formation of bed particle layers has often been suggested to be a prerequisite for bed agglomeration. In this work, the bed particle layer characteristics were found to differ between bed particles of different ages. On the basis of the experimental

results, processes responsible for layer formation are discussed below.

In BFB samples (BFB at 5 kW and BFB at 30 MW), only one layer around the quartz bed particles was observed for particles with an age of 1 day or shorter. The younger quartz bed particles, taken from both the 5 kW and 30 MW BFBs, have layers with a significantly higher K/Ca molar ratio than the older bed particles. The higher K/Ca ratio in the formed bed layers for the younger bed particles suggest that the initial step of the layer formation process starts with the formation of a K silicate melt produced via the reaction between the quartz bed particle surface and gaseous/condensed alkali species. This sticky surface will subsequently trap coarse fly ash particles produced from the fuel mainly consisting of refractory oxides, including CaO and MgO. Attached on the sticky/molten bed particle layer surface, these particles could subsequently dissolve into and react with the melt, thereby decreasing the K/Ca ratio in the layer. According to the ternary phase diagram K<sub>2</sub>O–CaO–SiO<sub>2</sub>, the lowest melting temperature occurs in compositions around 70 mol % Si and 30 mol % K,<sup>27</sup> while introducing increasingly more Ca moves the composition to areas with higher melting temperatures. The dissolution of calcium into the melt could also enhance the release of alkali from the melt.<sup>28,29</sup> Furthermore, Mg appears to be less reactive/soluble in the melt in comparison to Ca, because a higher Ca content was found in the inner layer rather than the outer coating layer and a higher Mg concentration was found in the outer coating layer (Figure 6b). This is in accordance with previously reported results in combustion of woody fuels.<sup>14</sup> During this early stage of the layer formation process, as discussed before, only one bed particle layer was observed, which indicates that ash particles attached on the bed particle surface could react relatively fast with the initially formed molten quartz bed particle layer. The dominating reaction during this stage is between K species and quartz.

Two layers consisting of a homogeneous inner layer and an inhomogeneous outer layer with compositions similar to fuel were found for BFB particles with age longer than 3 days. For bed particles from BFB30 with age from around 1 day to 13 days, the layer growth rate is initially relatively high but decreases over time. According to Figure 6a, the calcium concentration in the inner layer increases but the rate decreases over time, following the similar trend of the inner layer growth rate. The K/Ca molar ratio of the inner layer decreases from day 1 to day 5, most likely because of the diffusion of and reaction with CaO from the outer layer. For the inner layer composition, an obvious increase of Ca was found from 5 to 13 days (Figure 6a). Therefore, the K/Ca molar ratio keeps decreasing for bed particles with age from around day 1 to day 13 (Figure 8). However, with increasing amounts of dissolved CaO in the molten phase, the limit of saturation is approached; i.e., conditions for crystallization of CaSiO<sub>3</sub> (s) are reached.

For BFB30 samples from day 13 and day 23, the K concentration was very low, whereas the Ca/Si ratio reached a relatively high level. The calcium-rich silicate layer thus formed to an increasing extent “protected” the bed particles from further potassium attacks and subsequently significantly reduced the rate of the inner layer formation process. The molar ratios of Ca<sub>2</sub>SiO<sub>4</sub> and Ca<sub>3</sub>SiO<sub>5</sub> to CaSiO<sub>3</sub> were used to investigate the occurrence of dominating crystalline phases of inner bed layers as a function of the sampling time, as illustrated in Figure 10. An obvious increase was found over time until day 13. This is interpreted as if, after the initial

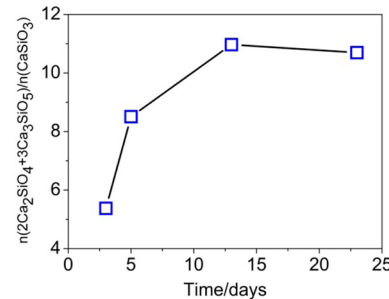


**Figure 10.** Molar ratio of the amount of element Ca in the chemical form of Ca<sub>2</sub>SiO<sub>4</sub> and Ca<sub>3</sub>SiO<sub>5</sub> to CaSiO<sub>3</sub> as a function of the sampling time.

crystallization of CaSiO<sub>3</sub>, the inner layer growth rate decreased significantly (see Figure 9b, around day 3 to day 23). Upon further supply of CaO from the outer layer, more CaO-rich silicates, such as Ca<sub>2</sub>SiO<sub>4</sub> and thereafter Ca<sub>3</sub>SiO<sub>5</sub>, were formed. Because these are solid-state and diffusion-controlled reactions, the continued layer formation rate was slow.

The results from SEM pictures show different layer morphologies between samples from CFB122 and BFB30. The outer coating layer is much thinner for CFB122 samples. The possible reason is that the outer coating layer formation rate is hampered because of the more significant attrition between particles in CFBs compared to those in BFBs. In that case, less calcium from the outer layer will be available to dissolve into the K-rich silicate melt that initially forms the inner quartz bed particle layer. Less Ca will thereby be available to decrease the amount of the molten phase in the inner bed particle layer, and potassium can go through the layer easily and react with the bed particle surface because of lower diffusion resistance. That can explain why higher K/Ca molar ratios in the inner layer for CFB samples compared to BFB samples collected after a similar time were observed.

In comparison to BFB particles of similar ages (3–6 days), the quartz bed particles of CFB samples had both more discontinuous inner layers and more cracks. These cracks were also found to propagate into the core of the quartz particle. The cracks of the inner layers could provide an additional route for the K species (g) to react with the bed particle surface, followed by dissolution/reaction of CaO (s). Thus, the inner–inner layer can usually be found where relatively thin inner layers or cracks are formed. Obviously, inner–inner layers with higher potassium and silicon contents and lower calcium content compared to inner layers can be observed for CFB samples (Figure 7). The formation of these inner–inner layers/core crack layers in older quartz bed particles has also been shown in other studies during wood combustion in CFBs using natural sand.<sup>30,31</sup> Because no cracks could be identified in the unused bed material, the formation of these cracks on older quartz bed particles remains unexplained. It has previously been speculated whether the phase transition between  $\alpha$  quartz and  $\beta$  quartz or quartz and tridymite can enhance the crack formation in the quartz bed particles because the molar volumes are different for all three phases.<sup>31</sup>

For woody fuels, the dominating elements in the quartz bed particle layers are calcium, silicon, oxygen, and potassium. The K/Ca and Ca/Si molar ratios of the (inner) layer as well as the layer growth rates were used to reveal/discuss the layer formation process. On the basis of that, the layer formation process could be divided into different stages. At an initial stage,

i.e., for bed particles with an age less than about 1 day, a high K/Ca molar ratio was observed. The layer formation process was dominated by the reaction of potassium with the quartz bed particle surface, and a relatively small quantity of the molten phase forms. Only one layer was formed during this stage. At the second stage (bed particles ages of 1–13 days), a substantial outer particle-rich layer was also formed and the K/Ca molar ratio of the inner bed particle layer decreased dramatically once plenty of Ca-rich coarse fly ashes attached on the sticky (partially melt) inner bed particle layer, providing a significant amount of calcium dissolving into the melt accompanied by a diminishing molten phase amount. During the initial days of this period, the layer growth rate was high but decreased over time. At the last stage (bed particles older than 13 days), the K/Ca molar ratio was low in the inner bed particle layer and remained constant during the sampling time, whereas the Ca/Si molar ratio was high. The dissolution rate of Ca became quite slow as a result of the quite low chemical driving force because no substantial molten phase was formed, resulting in a slow layer growth rate. In addition to these layer formation processes mentioned, an inner–inner/crack layer was also formed in CFB samples simultaneously with the inner bed particle layer. This layer was formed in the vicinity of formed cracks that were introduced already after some days in the CFB.

The practical implication of the results from this work is that a low bed material renewable rate in wood-derived fired BFB boilers using natural sand is recommended. The formation of high-melting Ca silicates for older quartz bed particles protects the bed particle layer surface from further attack of potassium, leading to reduced agglomeration tendency.

## 5. CONCLUSION

There were significant differences in layer morphology and composition for quartz bed particles with different ages. The K/Ca and Ca/Si molar ratios of the inner quartz bed particle layer were found to differ for samples with different sampling times. This has been used to depict different stages of the layer formation process.

At the initial stage of the quartz bed particle layer formation process, i.e., for bed particles with operational duration of less than about 1 day (24 h), only one thin Ca-, Si-, O-, and K-rich homogeneous layer that has a relatively high K/Ca molar ratio and slow layer growth rate was found. For bed particles with age from around 1 day to 2 weeks, also a substantial outer more particle (CaO) rich layer was found. During the initial days of this period, the layer growth rate is high but decreases over time, and decreasing K/Ca and increasing Ca/Si molar ratios in the inner bed particle layer were observed. For bed particles with age between 2 and 3 weeks, a much lower layer growth rate was observed. At the same time, the Ca/Si molar ratio reached high values and the K concentration remained on a very low level. In addition to these layer formation processes mentioned, also an inner–inner/crack layer with high K, Si, and O contents and relatively low Ca content was also formed in CFB quartz bed particles simultaneously with the inner bed particle layer. This layer was formed in the vicinity of formed cracks that were introduced already after some days in the CFB. The following coating/layer formation process is suggested:

The reaction of potassium species with the bed particle surface to form low-melting K-rich silicates is probably the first step in the buildup of a layer on bed quartz bed particles. The continuous layer growth could be induced by a gradual

incorporation of Ca into the melt, followed by the precipitation of stable and high-temperature melting calcium silicates. However, because of the increasing calcium concentration and release of potassium from the inner layer, the diffusion and reaction driving force for calcium decreases, resulting in a decreasing layer growth rate. The melting propensity of the inner layer could be an important factor on layer growth, because the presence of a molten phase promotes diffusion of Ca into the layer as well as reaction with the layer.

## ■ AUTHOR INFORMATION

### Corresponding Author

\*Telephone: +46-72-5117762. E-mail: hanbing.he@ltu.se.

### Notes

The authors declare no competing financial interest.

## ■ ACKNOWLEDGMENTS

Financial support from the Swedish Research Council (VR) is gratefully acknowledged.

## ■ REFERENCES

- (1) Elled, A. L.; Åmand, L. E.; Steenari, B. M. Composition of agglomerates in fluidized bed reactors for thermochemical conversion of biomass and waste fuels experimental data in comparison with predictions by a thermodynamic equilibrium model. *Fuel* **2013**, *111*, 696–708.
- (2) Grimm, A.; Skoglund, N.; Boström, D.; Eriksson, M.; Nordin, A. Bed agglomeration characteristics in fluidized quartz bed combustion of phosphorus-rich biomass fuels. *Energy Fuels* **2011**, *25* (3), 937–947.
- (3) Olofsson, G.; Ye, Z.; Bjerle, I.; Andersson, A. Bed agglomeration problems in fluidized-bed biomass combustion. *Ind. Eng. Chem. Res.* **2002**, *41* (12), 2888–2894.
- (4) Piotrowska, P.; Grimm, A.; Skoglund, N.; Boman, C.; Öhman, M.; Zevenhoven, M.; Boström, D.; Hupa, M. Fluidized-bed combustion of mixtures of rapeseed cake and bark: The resulting bed agglomeration characteristics. *Energy Fuels* **2012**, *26* (4), 2028–2037.
- (5) Boström, D.; Eriksson, G.; Boman, C.; Öhman, M. Ash transformations in fluidized-bed combustion of rapeseed meal. *Energy Fuels* **2009**, *23* (5), 2700–2706.
- (6) Chaivatamaset, P.; Sricharoon, P.; Tia, S. Bed agglomeration characteristics of palm shell and corncobs combustion in fluidized bed. *Appl. Therm. Eng.* **2011**, *31* (14–15), 2916–2927.
- (7) De Geyter, S.; Öhman, M.; Boström, D.; Eriksson, M.; Nordin, A. Effects of non-quartz minerals in natural bed sand on agglomeration characteristics during fluidized bed combustion of biomass fuels. *Energy Fuels* **2007**, *21* (5), 2663–2668.
- (8) Davidsson, K. O.; Steenari, B. M.; Eskilsson, D. Kaolin addition during biomass combustion in a 35 MW circulating fluidized-bed boiler. *Energy Fuels* **2007**, *21* (4), 1959–1966.
- (9) Brus, E.; Öhman, M.; Nordin, A. Mechanisms of bed agglomeration during fluidized-bed combustion of biomass fuels. *Energy Fuels* **2005**, *19* (3), 825–832.
- (10) Brus, E. Bed agglomeration during combustion and gasification of biomass fuels—Mechanisms and measures prevention. Ph.D. Thesis, Umeå University, Umeå, Sweden, 2004; ISBN: 91-7305-676-6.
- (11) De Geyter, S. Measures for preventing bed agglomeration using ash reaction chemistry. Licentiate Thesis, Umeå University, Umeå, Sweden, 2008; ISBN: 978-91-7264-707-7.
- (12) Öhman, M.; Pommer, L.; Nordin, A. Bed agglomeration characteristics and mechanisms during gasification and combustion of biomass fuels. *Energy Fuels* **2005**, *19* (9), 1742–1748.
- (13) Öhman, M.; Nordin, A.; Skrifvars, B. J.; Backman, R.; Hupa, M. Bed agglomeration characteristics during fluidized bed combustion of biomass fuels. *Energy Fuels* **2000**, *14* (1), 169–178.

- (14) Nuutinen, L. H.; Tiainen, M. S.; Virtanen, M. E.; Enestam, S. H.; Laitinen, R. S. Coating layers on bed particles during biomass fuel combustion in fluidized-bed boiler. *Energy Fuels* **2004**, *18* (1), 127–139.
- (15) Brus, E.; Öhman, M.; Nordin, A.; Boström, D. Bed agglomeration characteristics of biomass fuels using blast-furnace slag as bed material. *Energy Fuels* **2004**, *18* (4), 1187–1193.
- (16) Lind, T.; Valmari, T.; Kauppinen, E.; Nilsson, K.; Sfiris, G.; Maenhaut, W. Ash formation mechanisms during combustion of wood in circulating beds. *Proc. Combust. Inst.* **2000**, *28* (2), 2287–2295.
- (17) Zevenhoven-Onderwater, M.; Öhman, M.; Skrifvars, B. J.; Backman, R.; Nordin, A.; Hupa, M. Bed agglomeration characteristics of wood-derived fuels in FBC. *Energy Fuels* **2006**, *20* (2), 818–824.
- (18) Thy, P.; Jenkins, B. M.; Williams, R. B.; Lesher, C. E.; Bakker, R. R. Bed agglomeration in fluidized combustor fueled by wood and rice straw blends. *Fuel Process. Technol.* **2010**, *91* (11), 1464–1485.
- (19) Brus, E.; Öhman, M.; Nordin, A.; Skrifvars, B. J.; Backman, R. Bed material consumption in biomass fired fluidised bed boilers due to risk of bed agglomeration-coating formation and possibilities for regeneration. *IFRF Combust. J.* **2003**, 200302, 1–12.
- (20) Visser, H. J. M. *The Influence of Fuel Composition on Agglomeration Behaviour in Fluidised-Bed Combustion*; Energy Research Centre of the Netherlands (ECN): Petten, Netherlands, 2004; ECN-C-04-054.
- (21) Öhman, M.; Nordin, A. A new method for quantification of fluidized bed agglomeration tendencies: A sensitivity analysis. *Energy Fuels* **1998**, *12* (1), 90–94.
- (22) Bruker AXS GmbH. *Diffrac<sup>plus</sup>* EVA 10.0; Bruker AXS GmbH: Karlsruhe, Germany, 2003.
- (23) International Center for Diffraction Data (ICDD). *The Powder Diffraction File*, PDF-2; ICDD: Newtown Square, PA, 2004.
- (24) Bruker AXS GmbH. *Diffrac<sup>plus</sup>* TOPAS 2.1; Bruker AXS GmbH: Karlsruhe, Germany, 2003.
- (25) Fachinformationszentrum Karlsruhe (FIZ Karlsruhe). *Inorganic Crystal Structure Database Online (ICSD Web)*; FIZ Karlsruhe: Karlsruhe, Germany; <http://icsd.fiz-karlsruhe.de/>.
- (26) Liu, J.; Saw, R. E.; Kiang, Y. H. Calculation of effective penetration depth in X-ray diffraction for pharmaceutical solids. *J. Pharm. Sci.* **2010**, *99* (9), 3807–3814.
- (27) Morey, G. W.; Kracek, F. C.; Bowen, N. L. The ternary system K<sub>2</sub>O–CaO–SiO<sub>2</sub>. *J. Soc. Glass Technol.* **1930**, *14*, 149–187.
- (28) Gilbe, C.; Öhman, M.; Lindström, E.; Boström, D.; Backman, R.; Samuelsson, R.; Burvall, J. Slagging characteristics during residential combustion of biomass pellets. *Energy Fuels* **2008**, *22* (5), 3536–3543.
- (29) Thy, P.; Lesher, C. E.; Jenkins, B. M. Experimental determination of high-temperature elemental losses from biomass slag. *Fuel* **2000**, *79* (6), 693–700.
- (30) Latva-Somppi, J.; Kurkela, J.; Tapper, U.; Kauppinen, E. I.; Jokiniemi, J. K.; Johanson, B. *Proceedings of the International Conference on Ash Behavior Control in Energy Conversion Systems*; Pacifico Yokohama, Japan, March 18–19, 1998; pp 119–126.
- (31) Tranvik, A. C.; Öhman, M.; Sanati, M. Bed material deposition in cyclones of wood fuel fired circulating fluidized beds (CFBs). *Energy Fuels* **2007**, *21* (1), 104–109.